Highly directed emission from self-assembled quantum dots into guided modes in disordered photonic-crystal waveguides

T. Reichert,[1,2] S. Lichtmannecker,[1,2] G. Reithmaier,[1,2] M. Zeitlmair,[1,2] J. Wembacher,[1,2] A. Rauscher,[1,2] M. Bichler,[1,2] K. Müller,[1,2,3] M. Kaniber,[1,2,*] and J. J. Finley[1,2,†]

[1]*Walter Schottky Institut and Physik Department, Technische Universität München, Am Coulombwall 4, 85748 Garching, Germany*

[2]*Nanosystems Initiative Munich, Schellingstraße 4, 80799 München, Germany*

[3]*E. L. Ginzton Laboratory, Stanford University, Stanford, California 94305, USA*

(Received 24 July 2014; revised manuscript received 3 September 2014; published 24 September 2014)

We explore the dynamics and directionality of spontaneous emission from self-assembled In(Ga)As quantum dots into transverse-electric–polarized guided modes in GaAs two-dimensional photonic-crystal waveguides. The local group velocity of the guided waveguide mode is probed, with values as low as $\sim 1.5\%\, c$ measured close to the slow-light band edge. By performing complementary continuous-wave and time-resolved measurements with detection along and perpendicular to the waveguide axis, we probe the fraction of emission into the waveguide mode (β factor). For dots randomly positioned within the unit cell of the photonic-crystal waveguide, our results show that the emission rate varies from $\geqslant 1.55$ ns^{-1} close to the slow-light band edge to $\leqslant 0.25$ ns^{-1} within the two-dimensional photonic band gap. We measure an average Purcell factor of $\sim 2\times$ for dots randomly distributed within the waveguide and maximum values of $\beta \sim 90\%$ close to the slow-light band edge. Spatially resolved measurements performed by exciting dots at a well-controlled distance of 0–45 μm from the waveguide facet highlight the impact of disorder on the slow-light dispersion. Although disorder broadens the spectral width of the slow-light region of the waveguide dispersion from $\delta E_d \leqslant 0.5$ to >6 meV, we find that emission is nevertheless primarily directed into propagating waveguide modes. The ability to control the rate and directionality of emission from isolated quantum emitters by placing them in a tailored photonic environment provides much promise for the use of slow-light phenomena to realize efficient single-photon sources for quantum optics in a highly integrated setting.

DOI: 10.1103/PhysRevB.90.115310 PACS number(s): 42.50.Ct, 42.70.Qs, 78.67.Hc, 78.47.−p

I. INTRODUCTION

Many of the existing proposals for optically based quantum information technologies rely on the availability of efficient sources of single photons [1–3] and the ability to enhance the strength of light-matter interactions to a level where few photon nonlinearities appear in the optical response [4]. To date, such quantum optical nonlinearities have been demonstrated for several free-space and cavity-QED systems, including atoms in high-finesse optical resonators [5,6], semiconductor quantum dots (QDs) embedded within high-Q (Q = quality factor) solid-state nanocavities [7–11], and individual dye molecules subject to polychromatic excitation [12]. In light of these impressive demonstrations, several groups have already turned their attention to integrated geometries [4,13,14] whereby cavities, waveguides (WG), and quantum emitters can be combined on the same chip to realize new types of quantum sources [15]. High-Q photonic-crystal (PhC) defect cavities can be readily fabricated next to waveguides to effectively direct quantum light into propagating modes on a chip [16]. However, *in situ* frequency control is required to tune the QD emitter and cavity mode into resonance. In contrast, a broadband spontaneous-emission rate enhancement can be achieved using PhC waveguides close to the low group velocity (slow-light) regions of the dispersion relation for transverse-electric (TE)-guided modes [17–21] with measured coupling efficiencies of the emission to the waveguide mode approaching unity [22–25]. Moreover, a recent theoretical proposal [26] has indicated that the enhanced light-matter interaction close to slow-light modes in PhC waveguides may become sufficiently strong so as to result in single-photon nonlinearities. However, the low group velocity region of the propagating mode is inevitably impacted by disorder effects that can result in Anderson localization close to band edges [27–30], potentially hindering the practical use of slow-light phenomena.

In this paper, we combine continuous-wave (CW) and time-resolved photoluminescence (PL) spectroscopy to probe the coupling of QDs randomly distributed throughout a PhC $W1$ waveguide to the TE-polarized guided modes. We measure the local group velocity at specific points within the waveguide dispersion, obtaining values as low as $\sim 1.5\%\, c$ close to the band edge. This enables us to directly correlate the measured local spontaneous-emission rate with the spectrum of the radiation detected along two orthogonal axes: parallel to the waveguide axis and normal to the plane of the two-dimensional (2D) PhC. Our results show that the average spontaneous-emission rate varies from $\geqslant 1.55$ ns^{-1} for dots emitting close to the slow-light region of the waveguide dispersion to $\leqslant 0.25$ ns^{-1} within the 2D photonic band gap (PBG). For dots randomly positioned within the unit cell of the PhC waveguide, we measure a position-averaged Purcell factor up to $\sim 2\times$ and spontaneous-emission coupling factors into the guided waveguide mode up to $\beta \sim 90\%$. Finally, spatially resolved measurements directly elucidate the impact of fabrication disorder on the slow-light edge of the dispersion relation. We observe pronounced optical localization for random positions along the PhC waveguide. The slow-light waveguide mode

*kaniber@wsi.tum.de
†finley@wsi.tum.de

band edge is fluctuating over an energy interval $\delta E_d = 6$ meV due to the presence of disorder.

II. FABRICATION AND EXPERIMENTAL SETUP

The sample investigated was grown using molecular beam epitaxy on a 350-μm-thick [100] GaAs wafer. Growth began with a 800-nm-thick sacrificial layer of $Al_{0.8}Ga_{0.2}As$ grown on a 300 nm GaAs buffer, followed by a 150-nm-thick nominally undoped GaAs waveguide that contained a single layer of $In_{0.5}Ga_{0.5}As$ QDs at its midpoint. The growth conditions used for the QD layer are known to produce dots with an areal density $\rho_D \sim 50\ \mu m^{-2}$, emitting over the spectral range 1.24–1.40 eV. After growth, a hexagonal lattice of air holes was defined in a ZEP520A soft mask and deeply etched using a $SiCl_4$-based inductively coupled plasma to form a 2D PhC. By omitting a single row of air holes in the PhC lattice, we established a $W1$ waveguide that was subsequently cleaved to gain optical access via the side facet. As a final step, the AlGaAs layer was selectively removed with hydrofluoric acid to establish a free-standing membrane.

After fabrication, the sample was cooled to $T = 12$ K in a liquid-He flow cryostat for optical studies using a two-axis confocal microscope that facilitates the study of the optical response both perpendicular and parallel to the sample surface. The QDs were excited with a pulsed laser diode emitting at 1.9 eV (80 MHz repetition frequency, 70 ps pulse duration, Pico Quant, model P-650) along an axis normal to the plane of the waveguide. The signal was detected either via the same 50× objective (NA = 0.42), perpendicular to the plane of the PhC and waveguide axis, or from the side along the waveguide axis using a second 100× (NA = 0.5) objective. The diameter of the excitation spot was measured to be 1.3 μm such that ~50 QDs are excited directly. We spectrally dispersed the QD emission using a 0.5 m imaging monochromator and detected with a liquid-nitrogen-cooled CCD camera. For time-resolved measurements, a Si-avalanche photodiode was used, providing a temporal resolution of 350 ps.

Figure 1(a) shows selected scanning electron microscope (SEM) images of a structure that is nominally identical to the one used for optical studies. From such SEM images, we determined the air-hole radius to be $r/a = 0.315 \pm 0.005$, where $a = 250 \pm 2$ nm is the nominal periodicity of the PhC, the slab thickness $h = 150 \pm 5$ nm, and the waveguide length $l = 45 \pm 0.5\ \mu$m. Using the extracted geometrical parameters and the refractive index for GaAs of $n_{GaAs} = 3.5$, we performed three-dimensional calculations of the photonic band structure [32]. Selected examples of such calculations are presented in the leftmost panel of Fig. 1(b) and show the dispersion for TE-like modes along the Γ-K' direction in the first Brillouin zone [33,34]. The fundamental (zeroth-order) and first-order waveguide modes are labeled $WG\,0$ (black line) and $WG\,1$ (blue line), respectively, while the light-blue shaded region marks the light cone and the orange dashed line marks the position of the edge of the 2D photonic band gap. Clearly, the fundamental waveguide mode is expected to be guided in the spectral range $E = 1.296$–1.361 eV, below the light line, and the first-order waveguide mode from $E = 1.391$–1.439 eV, within the 2D photonic band gap.

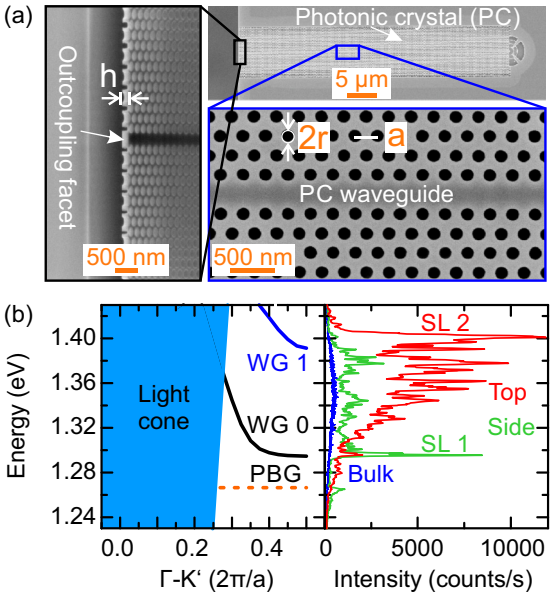

FIG. 1. (Color online) (a) Selected SEM images of one-half of the cleaved $W1$ PhC waveguide with a grating coupler on the opposite end [31], nominally identical to the sample used for the spectroscopic studies. The leftmost image shows the cleaved facet with the under-etched membrane, tilted at an angle of 60°. The rightmost images show planar views. From these images, the air-hole radius $r = 79 \pm 2$ nm, lattice constant $a = 250 \pm 2$ nm, and slab thickness $h = 150 \pm 5$ nm were determined. (b) Left panel: Photonic band structure calculation for the structural and geometrical parameters extracted from the SEM images shown in (a). The black and blue solid lines show the zeroth- and first-order waveguide modes, respectively. The orange dashed line marks the upper edge of the 2D photonic band and the light-blue shaded region represents the free-space light cone. In the rightmost panel, we present typical μ-PL measurements of the investigated structure excited at the position of the waveguide from the top (see text) and detected from the side (green) and top (red), respectively. The blue spectrum shows typical QD emission recorded from the top using identical conditions from the unprocessed region of the sample for comparison.

The rightmost panel of Fig. 1(b) shows typical QD PL spectra recorded by exciting a specific position on the waveguide 10 μm from the cleaved facet and detecting emission either from the facet (green spectrum) or normal to the plane of the waveguide at the excitation position (red spectrum). The blue spectrum shows a typical emission spectrum recorded using nominally identical conditions from the unprocessed region of the sample, with a near featureless form reflecting the comparatively large number of QDs excited. In contrast, the spectra recorded from the waveguide exhibit a narrow peak close to the slow-light region of the fundamental waveguide mode at $E_1^{SL} = 1.296$ eV, labeled SL_1 in Fig. 1(b). The energy of the peak SL_1 is in excellent agreement with our photonic band structure simulations and the feature is observed for both top- and side-detection geometries. Similarly, a weaker additional feature, labeled SL_2 in Fig. 1(b), is observed only for the top-detection geometry at $E_2^{SL} = 1.391$ eV. We identify SL_2 as arising from the first-order waveguide mode; its absence in the side-detection geometry is most probably a result of the higher propagation losses of the higher-energy waveguide

mode. The characteristic form of the emission spectrum clearly indicates that the tailored photonic mode density experienced by QDs strongly modifies the directionality of the spontaneous emission, as expected.

III. RESULTS AND DISCUSSION

In this section, we present a detailed study of the modified QD emission properties, the decreased group velocity, and the impact of disorder on the slow-light cutoff energy. To gain insight into the QD emission dynamics, we performed time-resolved PL measurements to directly probe the local photonic mode density experienced by the dots within the waveguide. The modified photonic mode density is expected to strongly influence the radiative decay rate according to the effective Purcell factor, which is given by

$$F_P = (3\pi c^3)/(A_{\text{eff}}\omega_{QD}^2\epsilon^{3/2})(1/v_g), \quad (1)$$

where A_{eff} is the effective mode area and $v_g = \hbar^{-1}(dE/dk)$ is the local group velocity of the waveguide mode [17]. The enhanced density of propagating modes close to the slow-light regions of the waveguide dispersion are expected to influence the directionality of the spontaneous emission. We measured the frequency dependence of the spontaneous-emission rate spanning the energy range between 1.225 and 1.395 eV, overlapping with the 2D photonic band gap and the waveguide modes. Hereby, we used the spectrometer as a spectral filter with a bandpass of 0.5 meV and recorded decay transients in steps of 2 meV via the waveguide facet with the excitation laser positioned on the waveguide 10 μm away from the facet.

Typical intrinsic decay rates for QDs within the unpatterned region of the GaAs membrane lie in the range 1–1.25 ns^{-1}, increasing monotonically toward higher emission energies presumably as a consequence of the large coherence volume in more strongly confined dots. In strong contrast, the spectral evolution of the measured emission rate from dots within the waveguide exhibits considerably more complex decay dynamics with a much richer spectral dependence. Typical representative data are presented in Fig. 2(a) for the excitation spot positioned ~10 μm from the waveguide facet and a range of different detection energies. A is outside the photonic band gap [blue trace, Fig. 2(a)], B is within the photonic band gap below the slow-light region of the waveguide dispersion [green trace, Fig. 2(a)], C is at the slow-light edge of the fundamental waveguide mode dispersion [red trace, Fig. 2(a)], and D is close to the guided, fast-light region of the fundamental waveguide dispersion [black trace, Fig. 2(a)]. Careful examination of the data presented in Fig. 2 shows that all decay transients can be well described by either mono- or biexponential fits of the form $I(t) = I_1[\exp(-t/\tau_1)] + I_2[\exp(-t/\tau_2)]$, respectively ($I_2 = 0$ for mono-exponential fits). The use of biexponential fits is motivated by the fact that we probe both spatially coupled and uncoupled QDs since the excitation spot is ~3× larger than the waveguide width. Furthermore, the slow component contains contributions from the recombination of dark excitons in the quantum dot [22,35,36]. In the photonic band-gap regime, a mono-exponential fit accounts best as there is only coupling to defect states introduced by the inductively coupled plasma etching [37].

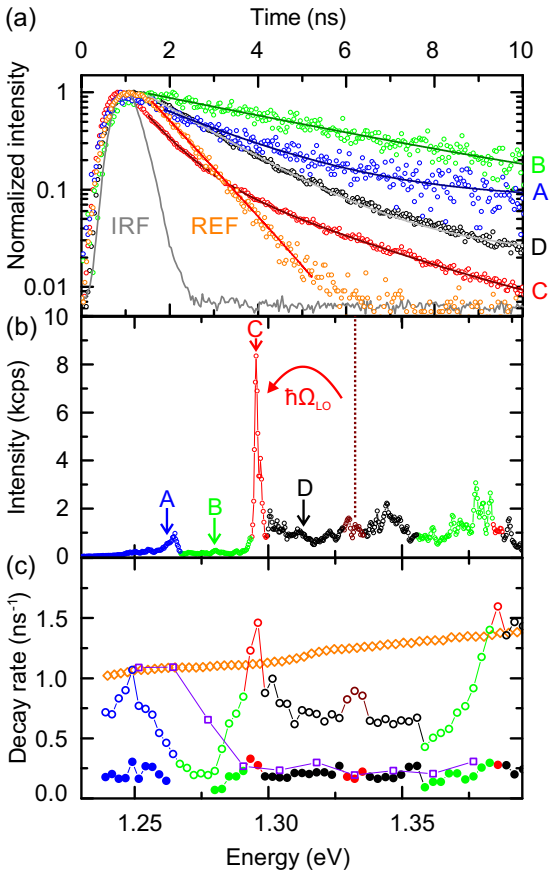

FIG. 2. (Color online) (a) Comparison of a typical decay transient recorded at a detection energy of ~1.3 eV from dots in the unpatterned region (REF) of the samples and selected decay transients (A,B,C,D) recorded at the spectral positions indicated in (b), using the measurement geometry described in the text (IRF: instrument response function). (b) Corresponding μ-PL spectrum detected from the side with top excitation 10 μm away from the facet. The slab band region is marked in blue, the photonic band gaps are green, the slow-light regions of the zeroth- and first-order mode are red, the fast-guided mode region is black, and the phonon-coupled slow-light region is brown. (c) Fast and slow spontaneous-emission rate of the QDs in the PhC waveguide as a function of the emission energy extracted from the decay transients as measured in (a) (open and closed circles, respectively). For comparison, the decay rate from QDs in the unprocessed region of the sample and on the PhC membrane away from the waveguide is shown by the orange and purple squares, respectively.

We now continue to discuss the form of these decay transients: Resonant with the slab mode continuum (A), we observe a biexponential decay from which we obtain a fast decay rate $\Gamma_1^{\text{Slab}} = 0.5 \pm 0.02$ ns^{-1} and a slow component $\Gamma_2^{\text{Slab}} = 0.25 \pm 0.02$ ns^{-1}. Inside the photonic band gap (B), however, we measure a mono-exponential decay and observe a significant decrease of the spontaneous emission rate to $\Gamma^{\text{PBG}} = 0.2 \pm 0.02$ ns^{-1}. In contrast, resonant with the slow-light region of the fundamental waveguide mode (C), we clearly observe again a biexponential decay transient with a fast component $\Gamma_1^{SL} = 1.55 \pm 0.3$ ns^{-1} and a slow component $\Gamma_2^{SL} = 0.37 \pm 0.02$ ns^{-1}. Finally, in the fast-guided mode

regime (D), we also find that a biexponential transient best accounts for the observed dynamics, extracting a fast decay rate $\Gamma_1^{FL} = 0.75 \pm 0.05$ ns^{-1} and a slow decay rate $\Gamma_2^{FL} = 0.17 \pm 0.01$ ns^{-1}. The corresponding μ-PL spectrum recorded from the side while exciting via the top is plotted in Fig. 2(b) for comparison. In Fig. 2(c), we present the extracted QD spontaneous-emission decay rate as a function of energy between 1.225 and 1.395 eV in steps of 2 meV. The open orange diamonds represent reference data obtained from dots outside a tailored photonic environment and the color-coded circles show the various decay rates measured from the $W1$ PhC waveguide. Whenever biexponential decay transients were observed, we plot the high and low decay rates, shown in Fig. 2(c) by open and filled circles, respectively. By comparing the measured QD decay rate inside the waveguide at the slow-light edge at $E_1^{SL} = 1.296$ eV with the reference decay rates in the unpatterned region of the sample at the same energy, we determine average Purcell factors between $F_P = 1$–2 for dots randomly positioned within the PhC unit cell, in good accord with expectations in the literature [23–25,38]. For the first-order waveguide mode, we observe a qualitatively similar behavior; however, it is far less pronounced, which we attribute to the lower group index as compared to the fundamental mode. Besides the maximum in the decay rate at the slow-light edge of the fundamental mode at $E_1^{SL} = 1.296$ eV, another weak peak is observed at 1.332 eV. The energy separation between these two features is very close to the GaAs longitudinal optical phonon energy ($\hbar\omega_{LO} = 36.6$ meV), indicative of a phonon-assisted QD-decay mechanism via the slow-light mode [39]. To estimate the fraction of photons coupled to the PhC waveguide mode (β_Γ factor), we also measured the spontaneous-emission rate for emission into the photonic band gap. The result is presented by the purple squares in Fig. 2(c), showing that typical decay rates for dots emitting into the photonic band gap are $\Gamma^{\mathrm{PBG}} = 0.22 \pm 0.02$ ns^{-1}. From the QD decay rates at the slow-light edge and the rates of QDs emitting into the photonic band gap at the same energy, we estimated the single-mode spontaneous-emission coupling factor β_Γ using

$$\beta_\Gamma = \frac{\Gamma_{WG}}{\Gamma_{WG} + \Gamma_{\mathrm{int}}}. \tag{2}$$

Here, Γ_{WG} is the QD decay rate into WG modes and Γ_{int} is the intrinsic emission decay rate in the photonic band gap [40]. Using the measured values of $\Gamma_1^{SL} = 1.55 \pm 0.3$ ns^{-1} and $\Gamma^{\mathrm{PBG}} = 0.2 \pm 0.02$ ns^{-1}, we estimate $\beta_\Gamma = 89 \pm 4\%$, in good agreement with previously published work [20,23,40,41].

Purcell factors up to ~30 have been theoretically predicted to be within reach for a group index as high as $c/v_g \sim 150$, corresponding to wave vectors close to the slow-light region of the waveguide mode ($k_{\Gamma-K} \sim 0.47\pi/a$) [41]. However, in experiments, an ideal spatial location of the emitter within the extended unit cell of the waveguide is crucial to reach these large values of F_P [41]. In order to estimate the expected Purcell factor of an ideally coupled QD emitting at $E_1^{SL} = 1.296 \pm 0.001$ eV, we measured the group index of the propagating waveguide mode [25] in PL measurements. Therefore, we excited with a high pump fluence (30 μW/μm^2), far above the QD s-shell saturation. Under such excitation conditions, the finite length of the PhC waveguide ($l = 45\,\mu$m)

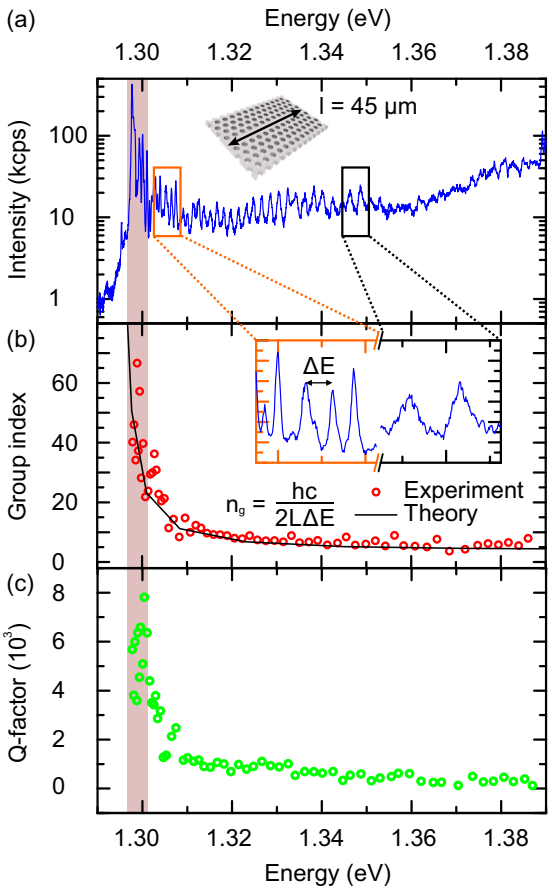

FIG. 3. (Color online) (a) High-power (30 μW/μm^2) μ-PL spectrum, detected from the side facet when exciting from the top 10 μm from the facet. (b) Group index as a function of energy. The red circles represent the group index extracted from measured data and the black solid line is the group index derived from the photonic band structure simulations presented in Fig. 1(b); the inset shows a zoom of (a). (c) Q factor extracted from (a) as a function of energy.

results in the appearance of clear Fabry-Perot oscillations in the waveguide emission. The local spacing of neighboring Fabry-Perot maxima are $\Delta E = hc/2n_gL$, where n_g is the mode group index and L is the length of the PhC waveguide. In Fig. 3(a), we present a typical high-power μ-PL spectrum, detected from the side facet while exciting from the top 10 μm away from the facet. Fabry-Perot oscillations are clearly observed with a continuous reduction of the mode spacing (from 2.5 down to 0.25 meV) when approaching the slow-light edge (red shaded region) from the high-energy side, reflecting the smaller group velocity when approaching the band edge [25]. From the data presented in Fig. 3, we calculated the group index n_g using

$$n_g = \frac{hc}{2L\Delta E}. \tag{3}$$

In Fig. 3(b), we present the extracted group index n_g as a function of energy. The group index clearly rises from ~5 to $\geqslant$70 when approaching the slow-light edge of WG 0. From this, we conclude that photons at the slow-light edge propagate along the waveguide at only 1.5% of the speed of light in vacuum. The calculated values extracted from

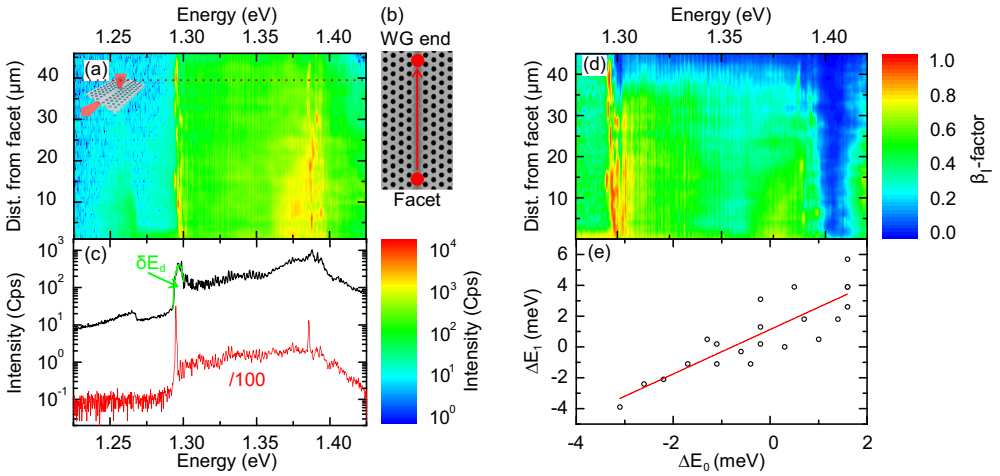

FIG. 4. (Color online) (a) Spectra recorded via the side channel as a function of the excitation position along the waveguide. (b) Top view SEM image from a waveguide identical to the measured one, illustrating the excitation spot scan. (c) Averaged spectrum of (a) (black curve) and a single spectrum when exciting 40 μm away from the facet [red curve; position is indicated by the red dotted line in (a)]. The two peaks in the single spectrum arise from the zeroth- and first-order mode. The slow-light disorder window width is $\delta E_d = 6 \pm 1$ meV. (d) Extracted β_I factor as a function of position and energy. (e) Disorder-induced mode peak deviation of mode 1 from the average as a function of mode peak deviation of mode 0 from the average.

the Fabry-Perot resonances are in very good agreement with the theoretical values obtained from the photonic band structure simulation (solid black line), confirming the accuracy of these simulations. Simultaneously, the Q factor of the Fabry-Perot resonances increases from a few hundred in the fast-light region of the waveguide dispersion up to ~8000 close to the slow-light edge, as shown in Fig. 3(c), reflecting the enhanced WG losses when approaching the light line.

We continue to explore the impact of disorder on the guided modes close to the slow-light edge of the waveguide mode. Figure 4(a) shows a false color image of PL spectra detected from the *side facet* when moving the excitation spot along the waveguide axis from the facet in steps of 1 μm [see Fig. 4(b)]. The spectra obtained clearly reveal a series of localized modes close to the slow-light edge $E_1^{SL} \sim 1.296$ eV, the energy at which fluctuations occur as the excitation spot is shifted along the waveguide. We identify such features as being due to disorder-induced localized modes close to the slow-light edge [27,28]. We note that the disorder-induced cavity-mode Q factors (~6000 to $\geqslant$8000) seem mainly to be limited by the in-plane optical confinement since photons still couple *primarily* to propagating waveguide modes, as demonstrated by the fact that we observe them most prominently in the side-detection geometry. To quantitatively estimate the impact of disorder on the slow-light cutoff energy, we compare in Fig. 4(c) the averaged spectrum of all positions shown in Fig. 4(a) (black curve) with a single spectrum detected from the side when exciting 40 μm away from the facet (red curve). For an individual spectrum, we observe a sharp resonance close to the energy of the slow-light edge at $E_1^{SL} = 1.296$ eV, similar in form to many of the spectra at different positions along the waveguide. In strong contrast, in the position-averaged spectrum, we observe a broadened peak at $\langle E_d^0 \rangle = 1.297$ eV with a full width at half maximum (FWHM) $\delta E_d = 6 \pm 1$ meV. This disorder bandwidth provides a measure of fabrication imperfections along the complete 45 μm length of the PhC waveguide. For a nominally identical waveguide, we measured an average radius fluctuation of ± 1 nm, which determines the lower limit of the disorder bandwidth. Additionally, hole position deviations, nonvertical sidewalls, and surface roughness might result in further increase of δE_d. Moreover, it has been shown that the disorder width can be artificially increased by randomly shifting the holes neighboring the PhC waveguide [42]. Furthermore, we investigated the impact of disorder on the β factor by recording both side- and top-detection signals *simultaneously*. We excite at a position distant x from the facet (data not shown) and define a quantity $\beta_I(\omega,x)$,

$$\beta_I(\omega,x) = \frac{\eta_{\text{side}} I_{\text{side}}(\omega,x)}{\eta_{\text{side}} I_{\text{side}}(\omega,x) + \eta_{\text{top}} I_{\text{top}}(\omega,x)} = \left[\frac{\eta_{\text{top}}}{\eta_{\text{side}}} \frac{I_{\text{top}}(\omega,x)}{I_{\text{side}}(\omega,x)} + 1\right]^{1/2}, \quad (4)$$

where $I_{\text{side}}(\omega,x)$ and $I_{\text{top}}(\omega,x)$ are the PL intensities detected from the side and top, respectively, and η_{side} and η_{top} are collection efficiencies in these two detection geometries. We assume η_{top} and η_{side} remain constant during the experiment and obtain $\eta_{\text{top}}/\eta_{\text{side}} \sim 0.22 \pm 0.07$. Using this result, we obtain a $\beta_I(\omega,x)$ factor using Eq. (4) and plot the result in Fig. 4(d). We observe a region around ~1.3 eV with β_I factors as high as $90 \pm 5\%$ which we identify to be the slow-light region of WG 0. Along the complete waveguide, we identify spatially localized hot spots with remarkably high β_I values, demonstrating that those spatial positions can be used to efficiently in-couple light into propagating waveguide modes. In the fast-guided region of the fundamental mode, we observe moderate β_I factors of $60 \pm 10\%$, which slightly decrease as the excitation spot moves away from the facet [green region of Fig. 4(d)]. In contrast, we identify decreased β_I factors of $10 \pm 5\%$ close to WG 1 around 1.40 eV, which we attribute to the pronounced losses due to scattering into

out-of-plane modes above the light line. Finally, we investigate if the influence of structural disorder simultaneously impacts both waveguide modes. Therefore, we define the energetic separation $\Delta E_0 = |E^0_{\rm dis} - \langle E^0_d\rangle|$ ($\Delta E_1 = |E^1_{\rm dis} - \langle E^1_d\rangle|$) of a disorder-induced localized state $E^{0/1}_{\rm dis}$ with respect to its according average $\langle E^0_d\rangle$ ($\langle E^1_d\rangle$) for the zeroth-order (first-order) mode. In Fig. 4(d), we plot ΔE_1 as a function of ΔE_0 for selected disorder-induced states distributed along the waveguide. We observe a strong correlation which is reflected by the linear fit and the Pearson-product-moment correlation coefficient is 0.86. However, the slope of 1.44 indicates that the fabrication-induced disorder has a larger impact on the first-order mode than on the fundamental mode.

IV. CONCLUSIONS

In summary, we explored the radiative coupling of InGaAs QDs to the modified photonic environment of zeroth- and first-order guided modes in PhC linear waveguides. The modified density of states in the PhC waveguide was found to have a strong influence on the directionality and rate of spontaneous emission. Average Purcell factors up to $\sim$2, β_Γ factors $\sim$90%, and group indices up to $n_g \sim 70$ were observed at specific locations along the waveguide axis. Moreover, the impact of disorder on the slow-light mode was evidenced by the observation of localized cavity modes randomly positioned along the WG axis with a frequency close to the slow-light mode. Here, disorder-induced localization resulted in high-Q modes that fluctuate with an energy bandwidth of $\delta E_d = 6$ meV around the slow-light band edge with Q factors up to $\sim$8000. Nevertheless, the most efficient radiative loss channel for the localized cavity modes was found to be radiation into propagating waveguide modes. Our results demonstrate that slow-light phenomena can be exploited for future integrated quantum circuits but that design tolerances must be able to account for the disorder-induced localization and, thereby, mechanisms to tune the local electronic and photonic properties would still be needed.

ACKNOWLEDGMENTS

Many thanks to V. Savona and M. Minkov for useful discussions and we gratefully acknowledge financial support from the DFG via Grant No. SFB-631 and the German excellence initiative via the Nanosystems Initiative Munich, the BMBF via Project No. 16KIS0110, part of the Q.com-Halbleiter consortium and BaCaTeC via the project Integrated Quantum Optics. T.R. additionally acknowledges support of the TUM-GS.

[1] E. Knill, R. Laflamme, and G. J. Milburn, Nature (London) **409**, 46 (2001).
[2] J. Claudon, J. Bleuse, N. S. Malik, M. Bazin, P. Jaffrennou, N. Gregersen, C. Sauvan, P. Lalanne, and J.-M. Gérard, Nat. Photon. **4**, 174 (2010).
[3] M. E. Reimer, G. Bulgarini, N. Akopian, M. Hocevar, M. B. Bavinck, M. A. Verheijen, E. P. A. M. Bakkers, L. P. Kouwenhoven, and V. Zwiller, Nat. Commun. **3**, 737 (2012).
[4] J. L. O'Brien, A. Furusawa, and J. Vučković, Nat. Photon. **3**, 687 (2009).
[5] Q. A. Turchette, C. J. Hood, W. Lange, H. Mabuchi, and H. J. Kimble, Phys. Rev. Lett. **75**, 4710 (1995).
[6] G. Nogues, A. Rauschenbeutel, S. Osnaghi, M. Brune, J. Raimond, and S. Haroche, Nature (London) **400**, 239 (1999).
[7] D. Englund, A. Faraon, I. Fushman, N. Stoltz, P. Petroff, and J. Vučković, Nature (London) **450**, 857 (2007).
[8] I. Fushman, D. Englund, A. Faraon, N. Stoltz, P. Petroff, and J. Vučković, Science **320**, 769 (2008).
[9] D. Englund, B. Shields, K. Rivoire, F. Hatami, J. Vuckovic, H. Park, and M. D. Lukin, Nano Lett. **10**, 3922 (2010).
[10] T. Volz, A. Reinhard, M. Winger, A. Badolato, K. J. Hennessy, E. L. Hu, and A. Imamoğlu, Nat. Photon. **6**, 605 (2012).
[11] D. Englund, A. Majumdar, M. Bajcsy, A. Faraon, P. Petroff, and J. Vučković, Phys. Rev. Lett. **108**, 093604 (2012).
[12] J. Hwang, M. Pototschnig, R. Lettow, G. Zumofen, A. Renn, S. Götzinger, and V. Sandoghdar, Nature (London) **460**, 76 (2009).
[13] T. Honjo, K. Inoue, and H. Takahashi, Opt. Lett. **29**, 2797 (2004).
[14] H. Takesue and K. Inoue, Opt. Express **13**, 7832 (2005).
[15] C. S. Muñoz, E. del Valle, A. G. Tudela, K. Müller, S. Lichtmannecker, M. Kaniber, C. Tejedor, J. Finley, and F. Laussy, Nat. Photon. **8**, 550 (2014).
[16] P. Yao and S. Hughes, Phys. Rev. B **80**, 165128 (2009).
[17] V. S. C. Manga Rao and S. Hughes, Phys. Rev. Lett. **99**, 193901 (2007).
[18] S. Hughes, Opt. Lett. **29**, 2659 (2004).
[19] E. Viasnoff-Schwoob, C. Weisbuch, H. Benisty, S. Olivier, S. Varoutsis, I. Robert-Philip, R. Houdré, and C. J. M. Smith, Phys. Rev. Lett. **95**, 183901 (2005).
[20] G. Lecamp, P. Lalanne, and J. P. Hugonin, Phys. Rev. Lett. **99**, 023902 (2007).
[21] Y. A. Vlasov, M. O'Boyle, H. F. Hamann, and S. J. McNab, Nature (London) **438**, 65 (2005).
[22] T. Lund-Hansen, S. Stobbe, B. Julsgaard, H. Thyrrestrup, T. Sünner, M. Kamp, A. Forchel, and P. Lodahl, Phys. Rev. Lett. **101**, 113903 (2008).
[23] H. Thyrrestrup, L. Sapienza, and P. Lodahl, Appl. Phys. Lett. **96**, 231106 (2010).
[24] S. Dewhurst, D. Granados, D. Ellis, A. Bennett, R. Patel, I. Farrer, D. Anderson, G. Jones, D. Ritchie, and A. Shields, Appl. Phys. Lett. **96**, 031109 (2010).
[25] T. Ba Hoang, J. Beetz, L. Midolo, M. Skacel, M. Lermer, M. Kamp, S. Hofling, L. Balet, N. Chauvin, and A. Fiore, Appl. Phys. Lett. **100**, 061122 (2012).
[26] J. Gao, F. Sun, and C. W. Wong, Appl. Phys. Lett. **93**, 151108 (2008).
[27] J. Gao, S. Combrie, B. Liang, P. Schmitteckert, G. Lehoucq, S. Xavier, X. Xu, K. Busch, D. L. Huffaker, A. De Rossi*et al.*, Sci. Rep. **3**, 1994 (2013).

[28] V. Savona, Phys. Rev. B **83**, 085301 (2011).
[29] S. R. Huisman, G. Ctistis, S. Stobbe, A. P. Mosk, J. L. Herek, A. Lagendijk, P. Lodahl, W. L. Vos, and P. W. H. Pinkse, Phys. Rev. B **86**, 155154 (2012).
[30] A. Lagendijk, B. van Tiggelen, and D. S. Wiersma, Phys. Today **62**, 24 (2009).
[31] A. Faraon, I. Fushman, D. Englund, N. Stoltz, P. Petroff, and J. Vuckovic, Opt. Express **16**, 12154 (2008).
[32] N. Savage, Nat. Photon. **1**, 598 (2007).
[33] S. G. Johnson, P. R. Villeneuve, S. Fan, and J. D. Joannopoulos, Phys. Rev. B **62**, 8212 (2000).
[34] D. Dorfner, T. Hurlimann, T. Zabel, L. H. Frandsen, G. Abstreiter, and J. Finley, Appl. Phys. Lett. **93**, 181103 (2008).
[35] J. M. Smith, P. A. Dalgarno, R. J. Warburton, A. O. Govorov, K. Karrai, B. D. Gerardot, and P. M. Petroff, Phys. Rev. Lett. **94**, 197402 (2005).
[36] J. Johansen, S. Stobbe, I. S. Nikolaev, T. Lund-Hansen, P. T. Kristensen, J. M. Hvam, W. L. Vos, and P. Lodahl, Phys. Rev. B **77**, 073303 (2008).
[37] H. Ryu, Y. Lee, R. Sellin, and D. Bimberg, Appl. Phys. Lett. **79**, 3573 (2001).
[38] A. Laucht, T. Günthner, S. Pütz, R. Saive, S. Frederick, N. Hauke, M. Bichler, M.-C. Amann, A. Holleitner, M. Kaniber, and J. Finley, J. Appl. Phys. **112**, 093520 (2012).
[39] U. Hohenester, A. Laucht, M. Kaniber, N. Hauke, A. Neumann, A. Mohtashami, M. Seliger, M. Bichler, and J. J. Finley, Phys. Rev. B **80**, 201311 (2009).
[40] A. Laucht, S. Pütz, T. Günthner, N. Hauke, R. Saive, S. Frédérick, M. Bichler, M.-C. Amann, A. W. Holleitner, M. Kaniber, and J. J. Finley, Phys. Rev. X **2**, 011014 (2012).
[41] V. S. C. Manga Rao and S. Hughes, Phys. Rev. B **75**, 205437 (2007).
[42] P. Garcia, A. Javadi, H. Thyrrestrup, and P. Lodahl, Appl. Phys. Lett. **102**, 031101 (2013).